Nozzle Tip Wetting in Gasoline Direct Injection Injector and Its Link with Nozzle Internal Flow

[1]Weidi HUANG, [1,2] Seoksu MOON, [3]Jin WANG, [4] Kei MURAYAMA, [5] Toshiyuki ARIMA, [6]Yuzuru SASAKI, [5]Akira ARIOKA*

[1]Research Institute for Energy Conservation, National Institute of Advanced Industrial Science and Technology, Ibaraki 305-8564, Japan.

[2]Inha University, 100 Inha-ro, Nam-gu, Incheon 22212, Republic of Korea.

[3]Advanced Photon Source, Argonne National Laboratory, Illinois, USA.

[4]Honda R&D Co., Ltd. Automobile R&D Center, Tochigi, 321-3393, Japan.

[5]Honda R&D Co., Ltd. Aircraft Engine R&D Center, Tochigi, 321-3393, Japan.

[6]Keihin Corporation. Tochigi Research & Development Center, Tochigi, 329-1233, Japan

**Corresponding Author: Seoksu Moon (E-mail address: ss.moon@inha.ac.kr))*

Abstract

Fuel film in the GDI Injector tip, or so-called nozzle tip wetting, has been found to be an important contributor of particle emissions. Attempts have been made to reduce the nozzle tip wetting by optimizing nozzle geometry designs. However, the inherent mechanism of the nozzle tip wetting formation and its link with nozzle internal flow is still unclear yet due to the lack of direct observations. To overcome this insufficiency, the nozzle internal flow and the formation process of the nozzle tip wetting were visualized in the real-scale aluminum nozzles using the X-ray phase-contrast technique. Results showed that the needle bouncing, injection pressure, and hole configuration affect the formation of the nozzle tip wetting, while the influence of needle bouncing is the most critical. A further study was conducted to examine the effect of nozzle counterbore diameter on the nozzle tip wetting. It was found that with an increase in counterbore diameter, the nozzle tip wetting slightly increased first and then decreased sharply after the counterbore diameter exceeded 0.40 mm. The mechanisms of the aforementioned phenomena were discussed in detail, which can contribute to the better understandings and control strategies of nozzle tip wetting.

Keyword: GDI engines, Particle emission, nozzle tip wetting, nozzle internal flow, needle motion

1. Introduction

Particle emissions from GDI engines have become a subject of concern. In the past emission regulations, particle emissions were considered as a matter of diesel engines only. In recent years, experimental evidence has shown that GDI engines may release more particle numbers (PN) than those of diesel engines in testing cycles and real driving conditions [1-3]. Consequently, the European emission regulations have started to limit

PN also for gasoline vehicles since 2014 [4]. In 2016, China has also announced its new emission standards with a requirement of limiting the PN emission applying to light-duty vehicles and taking effect beginning on July 1, 2020 [5].

To comply with increasingly stringent emission regulations, the controlling particle emissions of GDI engines has become a challenging issue [6-9]. The gasoline particulate filters (GPFs) has been considered seriously as one of the essentials in GDI engines to meet the emission standards. However, investigations have presumed that particle emissions might be controllable by the improved designs of the injector nozzle, and fuel film in the GDI injector tip otherwise known as the nozzle tip wetting has been found to be an important contributor of particle emissions [10-11]. There are two pathways that the nozzle tip wetting has been considered to affect particle emissions. First, experiments have suggested that when the flame front of the main combustion reaches the injector, the wetting fuel on the injector nozzle tip and in the counterbore could result in diffusion flame due to the local rich air/fuel mixture [12]. This phenomenon, regarded as the tip sooting, could contribute to the increased particle emissions. Second, injector deposit precursors are easily produced because of the uncompleted combustion of the tip-wetting fuel [13-15]. The presence of injector deposits is able to absorb and store more fuel during and after injection, leading to the even higher particle emissions [15]. Moreover, injector deposits could cause the injector fouling eventually, which changes the supplying fuel flow rate and spray pattern significantly in some cases, resulting in the further increased particle emissions. As a result, reducing the nozzle tip wetting is one of the keys to controlling the particle emissions in GDI engines.

Studies have shown that the nozzle tip wetting mainly depends on the flow conditions inside the nozzle hole and counterbore, which further relates to fuel properties, nozzle geometries, injection pressures, and nozzle temperature conditions [16-20]. It was reported that increasing injection pressures could improve PN emissions through reduced tip wetting [18]. *Oh et al*. reported that a decreased counterbore surface area could reduce the nozzle tip wetting effectively [19]. *Fischer et al*. mentioned that rising fuel temperatures can lead to a reduction in the nozzle tip wetting [20]. Although many parameters have been examined, the formation mechanism of tip wetting and the influencing mechanism due to the parameter changes have been rarely discussed yet. This insufficiency is mainly because of the lack of an experimental investigation to visualize the internal flow and nozzle tip wetting behavior simultaneously.

The flow characteristics inside engine nozzles are inaccessible for the measurements using the conventional light sources. Many attempts to visualize the nozzle internal flow have been conducted in the modeling nozzles, which either have a different nozzle dimension or are studied in the very different boundary conditions from

engine nozzles. It has made difficult to derive the clear understandings of phenomena in engine nozzles through the results of modeling nozzles. To overcome the above uncertainty, the X-ray phase-contrast imaging technique was applied in this study to ensure direct observations of the flow characteristics both inside and outside the nozzle. The nozzle tip-wetting phenomenon was examined in the real-size aluminum nozzles under the practical injection conditions of GDI engines. The effects of counterbore diameter on the nozzle tip wetting were further investigated. It was expected that the results obtained in this study can provide comprehensive understandings of the formation mechanism of the nozzle tip wetting and its control strategies.

2. Description of Experiments

2.1 X-ray Phase-Contrast Imaging

When X-rays pass through an object, not only X-ray amplitude but X-ray phase is altered. According to an ideal simulation, the phase-shift of an X-ray beam propagating through an object is much larger than the loss in intensity thus making the phase-contrast imaging more sensitive to the density variations in the object than absorption imaging [21]. This advantage could well contribute to imaging of the fuel injection process in the near-nozzle field and to the revealing of the perturbations in fuel structures during breakups. The propagation based phase-enhanced x-ray imaging was used in this study, which setup is very simple and basically the same as conventional radiography. The only difference is that the detector is not placed immediately behind the sample, but in some distance, so that the interference patterns between diffracted and undiffracted beam can be recorded [22]. Our experiments were performed at the 7ID-B station at Advanced Photon Source (APS), where provides a synchrotron X-ray source having the features of high brilliance, high collimation, and multiple pulse-selections. Owing to the high brilliance of the synchrotron X-ray beam, the imaging of fuel injection in a hundred-kilohertz rate with up to one-micrometer spatial resolution is achieved.

2.2 Experimental setup

Figure 1(a) shows the experimental setup in current study that resembles the one described in many of our previous investigations [23-26]. In the hybrid-fill beam mode of APS, a single bunch containing 16 mA isolated from the remaining bunches by symmetrical 1.594 microseconds gaps. The remaining current is distributed in 8 group of 7 consecutive bunches with a maximum of 11 mA per group, a periodicity of 68 ns, and a gap of 51 ns between groups, as presented in Figure 1(b). To protect the imaging system from the heat-load of X-ray beams, a mechanical shutter is used to ensure that X-ray beams pass through the shutter only at the imaging instant (8 ms opening duration). X-rays after penetrating through the sprays are converted to visible light using

a scintillator crystal (LuAg:Ce), which is then reflected by a 45° mirror and captured by a high-speed camera (Model SA-Z, Photron Inc.). In this study, the single bunch of the hybrid-fill beam mode was adopted for imaging because it provides a sufficiently high time resolution (150 ps). The camera frame rate was fixed to 67889 Hz (one-fourth of the revolution frequency of the electron bunches in the storage ring) as regards a compromise between a wide view field and a fast frame rate.

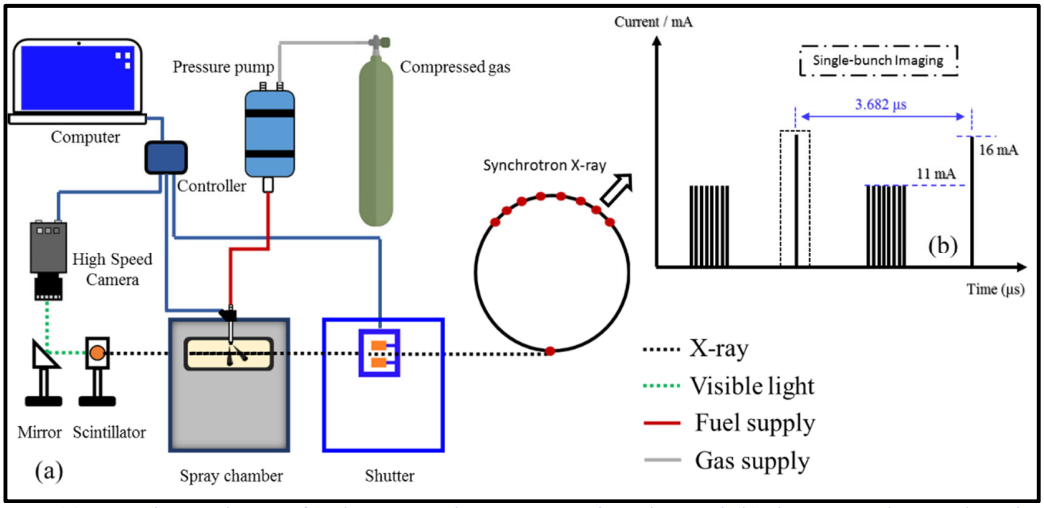

Figure 1. (a) Experimental setup for the X-ray phase-contrast imaging and (b) the X-ray electron bunches pattern of the hybrid mode in APS.

2.3 Experimental nozzles

In this investigation, the GDI nozzles made by the aluminum were used. The nozzle holes and counterbore were made by drilling and without abrasive flow manufacturing (AFM). Using the aluminum nozzles ensures the sufficient image brightness to visualize the flow inside the nozzle due to its higher X-ray transmittance compared to the stainless nozzles while keeping the similar performance in terms of the metal surface as well as sufficient strength to endure engine-like pressure. These nozzles have only two holes, and the holes have a different configuration, as seen in Figure 2. The counterbore diameter effect was discussed in this study using seven nozzles in total. The counterbore diameter of these nozzles is varied with a step of 0.05mm from 0.25 mm to 0.55 mm. Detailed descriptions of the nozzle geometries can be found in Table 1.

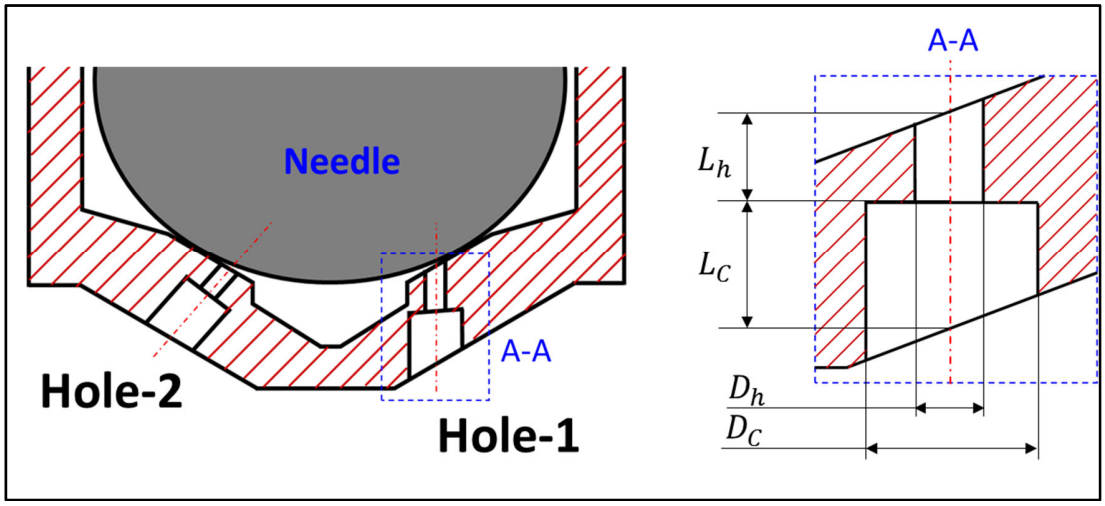

Figure 2. The nozzle internal structure and the definitions of the geometric parameters.

Table 1. Geometric parameters of test nozzles

Nozzle hole	Hole Diameter (D_h / mm)	Counterbore Diameter (D_c / mm)	Hole length (L_h / mm)	Counterbore length (L_c / mm)
Hole 1	0.16	0.25 ~ 0.55, 0.05/ step	0.26	0.35
Hole 2	0.16		0.18	0.42

2.4 Analysis method

The quantitative analysis was conducted as regards the needle motions, the flow separations in nozzle hole and the projected area of the nozzle tip wetting. With these results, the tip wetting formation and its influencing parameters are discussed. The definitions and calculations of these parameters are described below.

Needle Motions

The needle lift can be obtained using the cross-correlation analysis. The calculation process is described below. First, a raw needle image before injection was selected as the base image. A region of interest covering the needle tip (base window) was set in the base image, standing for the initial needle location. Second, a searching window having the same size as the base window was set in the needle image to be calculated (at a different timing, regarded as the calculation image). The similarity factor (r) between the images cropped from these two windows could be obtained using the two-dimensional cross-correlation calculation, as equation (1).

$$r = \frac{\sum_m \sum_n (A_{mn} - \bar{A})(B_{mn} - \bar{B})}{\sqrt{(\sum_m \sum_n (A_{mn} - \bar{A})^2)(\sum_m \sum_n (A_{mn} - \bar{A})^2)}} \quad (1)$$

where A and B are the croped images of the based window and the searching window, respectively, which have a image size of $m \times n$. $\bar{A}$ and $\bar{B}$ stand for the averaged grey value of A and B. This similarity factor was relevant to the location of the searching window, and its maximum would appear at where the cropped image from the searching window perfectly matched with that cropped from the base window. Then, the needle lift and wobbling could be derived based on the displacement of the search window relative to the base window. The details on needle motion can also refer to our previous studies [27, 28].

Flow separations

In this study, the flow separations inside the nozzle hole have been observed. To quantify the characteristics, an imaging processing method and calculation were used. Firstly, a background normalization together with the contrast adjustment was applied to the raw images of the nozzle internal flow, as shown in Figure 3(a). Then, the images at the steady state of injection and between shots were averaged as equation (2).

$$I = \sum_{shots} \sum_{t_1}^{t_2} I(t) \times \frac{1}{shots} \times \frac{1}{n}, \quad [t_1 = 1.0\ ms\ t_2 = 2.0\ ms] \text{ and } shots \text{ equal to } 5. \tag{2}$$

where n stands for the number of images within the steady state (1.0 ms – 2.0ms). Finally, in the processed image I, the profiles of flow separation were measured manually at different locations along the hole axis, as shown in Figure 3(b) and (c). It should be explained that the flow separation fluctuates slightly during the injection. Hence, the current method of measurement was used to guarantee the reliability of the results.

Projected area of the nozzle tip wetting

The characteristics of the nozzle tip wetting were quantified by examining its projected areas in the imaged direction. It should be explained that the holes of GDI nozzles normally are concentrated to the center of nozzle sac, and it can be observed that tip wetting occurs mostly at the nozzle exit. As a result, the projected area of tip wetting can be regarded proportional to the practical tip wetting amount, and thus using the projected area might as well ensure a valid examination of the tip wetting characteristics in this study. The calculation of the projected area of tip wetting is described below. Firstly, similar to the flow-separation detection, the raw images were processed by a background normalization together with the contrast adjustment, as seen in Figure 3(d) and (e). Then, the normalized image was further converted to a binarized image with an identical threshold applied for all the nozzles, as shown in Figure 3(f). Tip wetting was highlighted as the white region at the hole exit, and a consistent trend can be confirmed by comparing the images of Figure 3(e) and (f). At last, tip wetting area can be calculated by multiplying the total pixel numbers of the white region in Figure 3(e) with the pixel resolution. In this study, the imaging setup with an image resolution of 2.53 μm per pixel was achieved.

In addition, it might be of conern that a white fringe appeared at the liquid surface due to the phase contrast mechnism, which can affect the boundary definition of the tip wetting fuel. It is confirmed that the white fringe thickness is almost the same regardless of the tip wetting amount, This might be because a short sample-to-lense distance (30cm) is used in this study, where the phase contrast is relatively weak. Besides, the same threshold have beed applied to define the fuel boundary of tip wetting during image processings, and multiple-shots averaged results have been used for discussions.

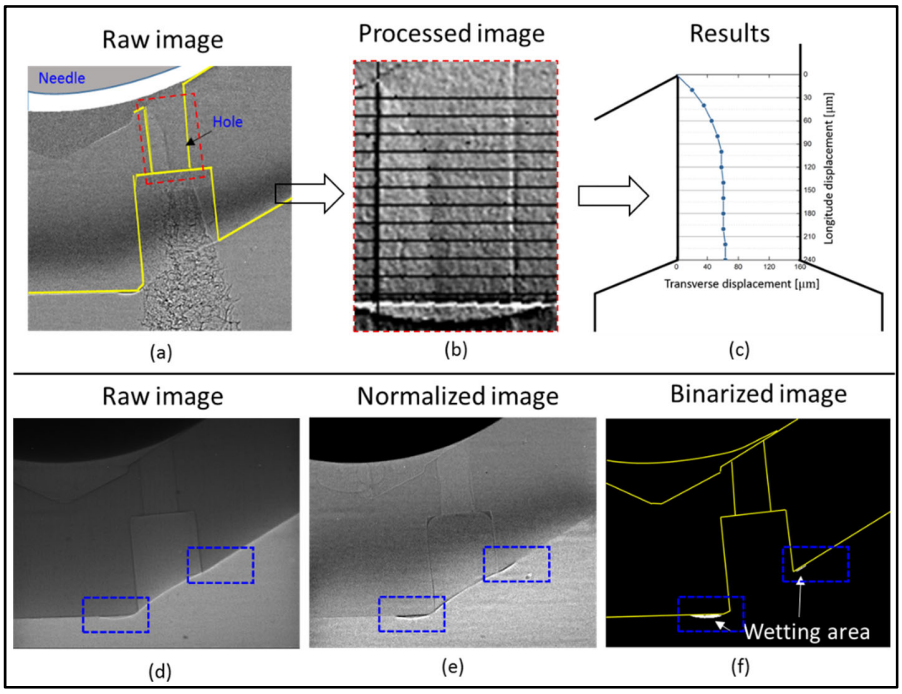

Figure 3. parameter definitions and calculation methods. (a-c) stand for a calculation of flow separation, while (d-f) show the calculation of the nozzle tip wetting area.

2.5 Experimental conditions

The experimental conditions were summarized in Table 2. Three different injection pressures were used to examine the injection pressure effect on tip wetting, including the injection pressures of 40 bar, 100 bar, and 200 bar. The spray chamber was filled with Nitrogen. The ambient gas pressure and temperature in the spray chamber were fixed to the atmospheric and room condition, respectively. The injection-pules duration was 2 ms and N-heptane was used instead of gasoline in consideration of the experimental safety. N-heptane has a similar surface tension value with gasoline that is very important regarding the tip wetting investigation. Another reason for utilizing n-heptane is because n-heptane has been historically used as a representative of the

n-alkane group due to its octane number and its concentration in gasoline fuel gasoline, which can mimic the combustion characteristics of gasoline fuel, especilly in low-temperature combustion regime [29]. This feature can also benefit to a link with the low-temperature combustion study in engines. Measurements were repeated five times at each testing condition and the shot-averaged results were obtained for the analysis below.

Table 2. Experimental conditions.

Injection (bar)	40, 100, 200
Ambient gas pressure (bar)	1.0
Ambient gas temperature (K)	Room condition (298)
Ambient gas density (kg/m^3)	1.25 kg/m^3 (N_2)
Fuel	n-heptane
Injection pulse (ms)	2.0 ms

3. Results and Discussions

3.1 Needle motion of test nozzles

Figure 4 shows the needle-motion results. These results are averaged between shots and the error bars are presented as well. Several features are evident in Figure 4. First, it is clear that the error bars are short, indicating good repeatability of the nozzle needle motion between shots. Second, Figure 4(a) and (b) show that the needle motions are slightly different among the nozzles as regards the height of the initial lifting peak, at the steady state, and at the end of injection. There is not a clear pattern linking the needle-motion differences to counterbore diameters so that the difference is considered to result from manufacturing tolerance. More discussions can be found in section 3.2.2. Third, the needle bouncing at the end of injection is observed in the nozzles with a similar amplitude. Most of the nozzles bounce twice during needle closing. Fourth, Figure. 4(c) and (d) reveal that increasing injection pressures result in a higher needle-lift height at the steady state. In addition, the needle lift declines slightly faster at higher injection pressures, however, the needle-bouncing amplitude becomes smaller. This phenomenon may result from that the higher injection pressure could press the upper part of the needle tip with a stronger force so that the needle closes faster and the afterward needle bouncing attenuates. The injection-pressure effect is consistent in the nozzles.

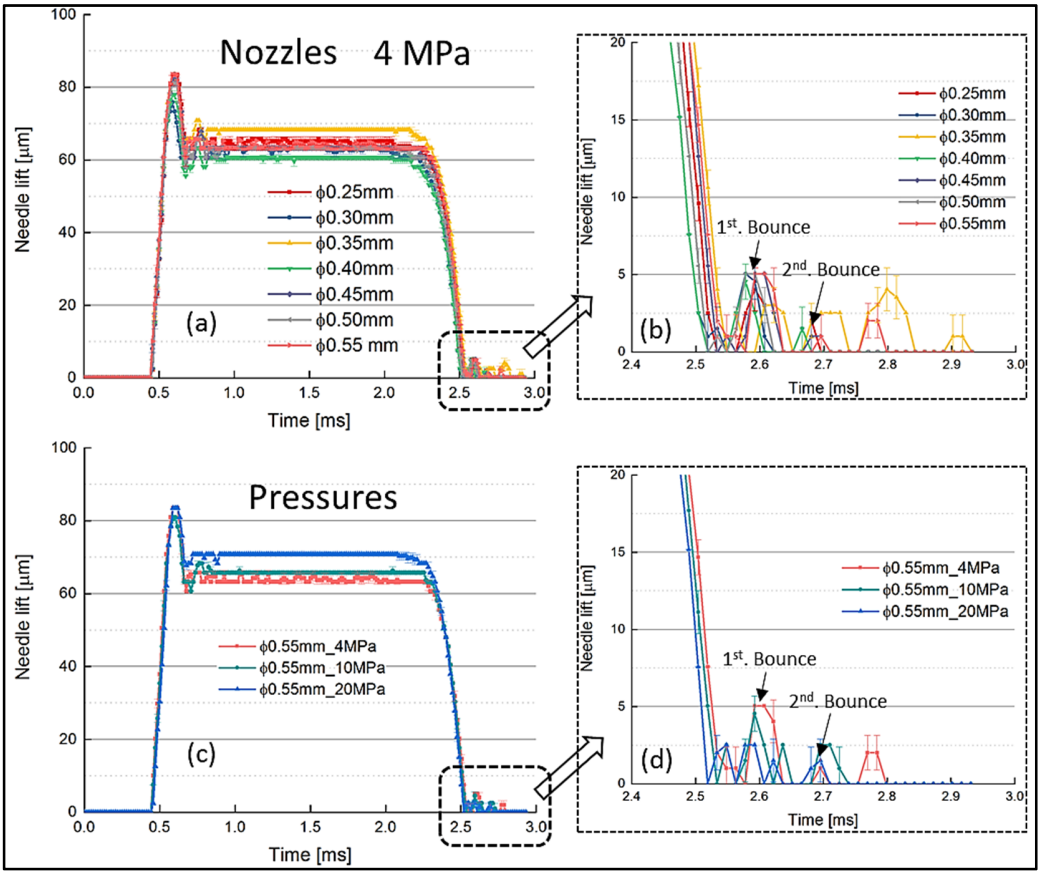

Figure 4. The results of needle motion. The counterbore diameter effect was presented in a full injection event as (a) and focused at the end of injection as (b), while the injection pressure effect was presented in a full injection event as (c) and focused at the end of injection as (d).

3.2 Nozzle tip wetting characteristics

3.2.1 Effects of needle motion, injection pressures, and hole configuration

Nozzle tip wetting results are presented in this section. Figure 5 shows the formation process of tip wetting with the images shown at different needle lifts. The 'first close' in Figure 5 means the time when the needle-lift height declines to zero before the 1st needle bouncing. The results shown below come from the nozzle with a counterbore diameter of 0.3 mm. The identical result trend can be found in the other nozzles as well. First, it is found that the nozzle tip wetting in Hole-1 appears soon after the beginning of injection, while interestingly in Hole-2 the nozzle tip wetting does not appear until the needle-bouncing period. A large number of fuel drippings come out during the needle-bouncing period in both nozzle holes. Hole-1 has a much severer tip wetting compared to Hole-2.

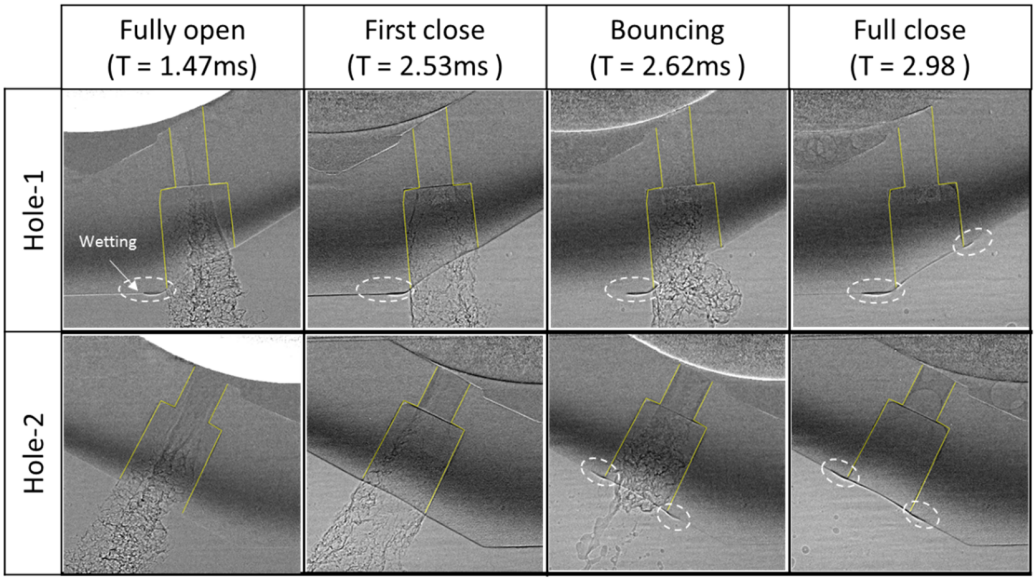

Figure 5. The nozzle tip wetting at the different needle lifts. Results from the nozzle with a counter diameter of Ø0.30 mm and under an injection pressure of 4 MPa are presented as a sample.

A quantitative analysis of the aforementioned phenomenon was conducted as regards the projected tip-wetting area at the nozzle exit. Figure 6(a) shows that the tip-wetting amount of Hole-1 increases gradually during injection, then decreases as the needle is declining, and sharply increases again during needle bouncing. It might be of particular interest that the nozzle tip wetting decreases when the needle is declining, and this phenomenon can be observed in all the nozzles. A discussion on this will be presented later. After the needle is fully closed (the needle bouncing is terminated, when is approximately 2.7 ms in Figure 6), the nozzle tip wetting still keeps increasing but much slower compared to that during needle bouncing. The higher injection pressures result in the less tip wetting, as shown in Figure 6(b). The nozzle tip wetting during the injection happens in Hole-1and under the injection pressure of 4 MPa only. The tip-wetting amount of Hole-1 is approximately three times larger than that of Hole-2. The results above indicate that the needle bouncing, injection pressure, and hole configuration affect the formation of tip wetting, while the influence of needle bouncing is the most critical.

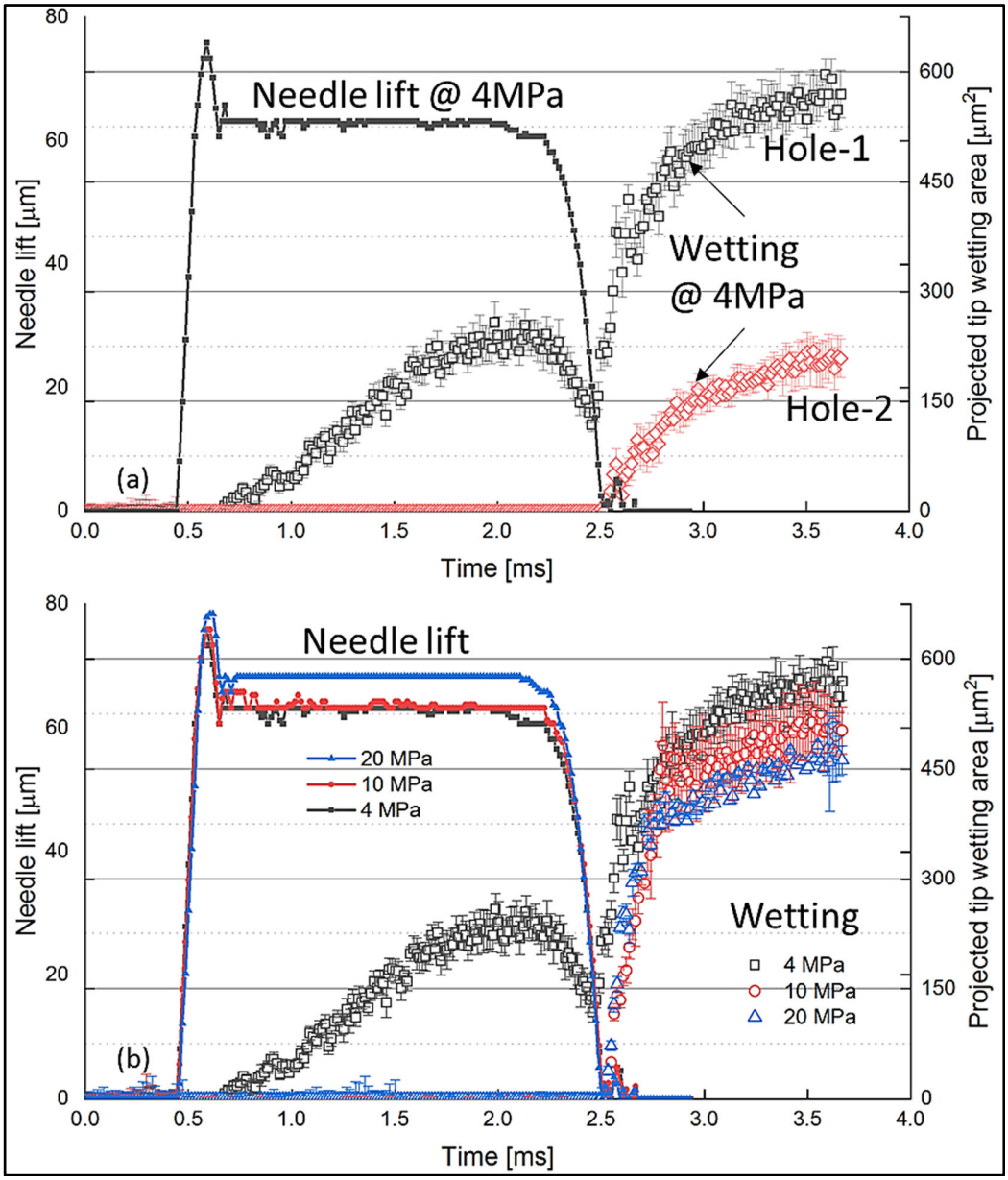

Figure 6. Results of the projected tip-wetting area. Results are compared between the Hole-1 and Hole-2 as (a), while (b) presents the results between different injection pressures from Hole-1. Ø0.30mm nozzle is used here standing for the identical trend within the nozzles.

Several observations in Figure 6 deserve further examinations. First of all, it is found that the needle bouncing has the most significant effect on tip wetting. To clarify this influence, Figure 7 reveals the detailed process with the images shown in a time sequence. It is found that after the needle is closed (Timing-1 to-3), fuel still flows down along counterbore walls, resulting in the first increase of the nozzle tip wetting. This can be

understood because, at the instance of the initial needle close, the pressure in nozzle sac is still higher than the ambient outside the nozzle. The pressure differential pushes out the residual fuel in nozzle sac making tip wetting increase. During the 1st needle bouncing (Timing-3 to-5), the spray-like fuel drippings appear with a large amount which are quite dispersive so that they touch counterbore walls and increase tip wetting significantly. During the 2nd needle bouncing (Timing-6 and after), the ligament-like fuel drippings appear, which incline to the right side in Hole-1, and attach to the counterbore wall in some shots. This can further increase tip wetting.

The needle bouncing effect could be as well responsible for the reduced tip wetting in high injection pressure conditions. As described earlier, the amplitude of needle bouncing attenuates as an increase in injection pressures, contributing to a reduced tip wetting. Besides, at high injection-pressures, it is argued that fuel drippings have relatively larger momentum to overcome the surface-tension effect against counterbore walls. This may also reduce tip wetting. The injection pressure effect on tip wetting can be explained based on these considerations.

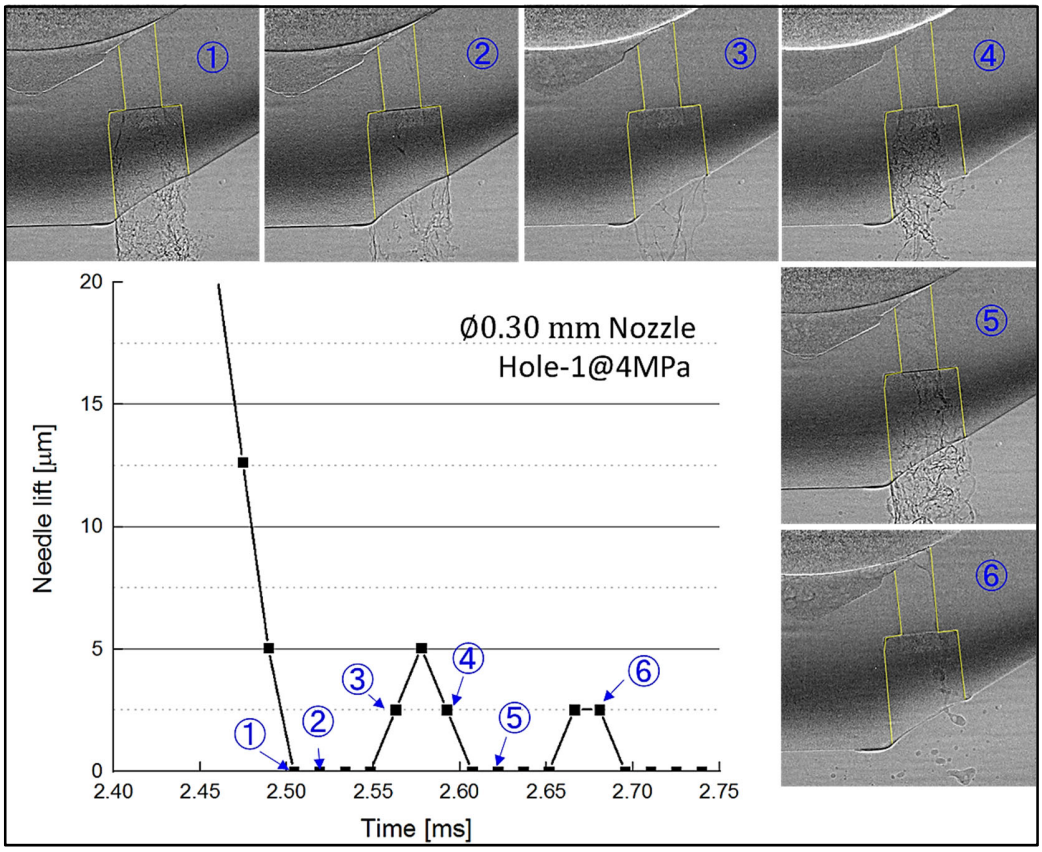

Figure 7. Needle-bouncing effect on tip wetting. (Ø0.30mm nozzle under 4 MPa)

It is found that the nozzle tip wetting of Hole-2 is much smaller than that of Hole-1. The reasons for this are considered separately during injection (means the steady-state, 1.0 ms – 2.0 ms) and at the end of injection (means from Timing-1, about 2.5 ms in Figure 7). First of all, during injection, tip wetting occurs in Hole-1 only. Figure 8 shows the flow separation profiles derived from the time-average results at the steady-state (1.0 ms – 2.0 ms). It is clear that there is a larger and single-sided flow separation in Hole-1 with an asymmetrical spray spreading in its counterbore, while Hole-2, by contrast, has a smaller and both-sided flow separations with the continuous and clear spray boundaries inside the counterbore. Our previous measurements have revealed that the spray velocity is much lower on the flow separation side (left side in the image) compared to that on the opposite side (right side in the image). In addition, *Itaya et al*. have reported in their numerical investigation that the flow separation enables the air entrainment backward to nozzle hole, which enhances flow turbulence resulting in the generation of small-size droplets on the flow separation side [30]. Based on these considerations, it is argued that the larger flow separations in Hole-1 benefit the formation of the small-size and low-velocity droplets that can be easily trapped on the counterbore wall under the surface-tension effect. As a result, the nozzle tip wetting during injection is observed in Hole-1. On the other hand, increasing injection pressures can ensure the sprays and droplets inside the counterbore having larger momentum to overcome the surface tension and to flush the impinging fuel out. Consequently, the tip wetting during injection occurs only in Hole-1 and under the injection pressure of 4 MPa.

In addition, it is found that tip wetting decreases when the needle is declining in Figure 4. It has been observed that the flow separations fluctuate more and become smaller during needle declining compared to that at the steady state. This phenomenon should be because of the enhanced flow turbulence when the needle is closing. As explained earlier, the smaller flow separations could reduce the generation of small-size droplets thus making tip wetting become less.

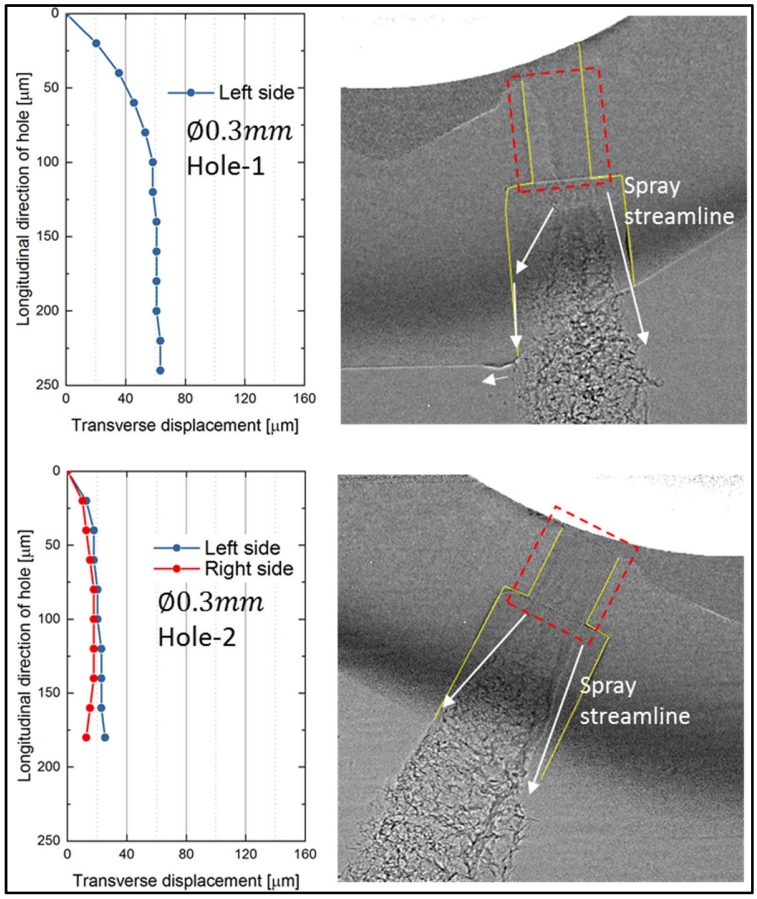

Figure 8. Comparisons of flow separation between Hole-1 and Hole-2. The flow separation results are shown on the left side, while two sampling images are presented on the right side. Results under an injection pressure of 4 MPa are used as a sample.

Furthermore, at the end of injection, tip wetting is found both in Hole-1 and Hole-2, but it increases more sharply in Hole-1. The reason for this can be explained with the images shown in Figure 9 (The 'Timing-4' in the figure equals to that shown in Figure 7). It can be seen that during needle bouncing, the spray-like fuel drippings appear both in Hole-1 and Hole-2. However, a larger dispersion of fuel drippings is observed in Hole-1, which increases the tip-wetting amount apparently as seen in Figure 9(b) and (c). The fuel drippings in Hole-2 mostly maintain a continuous boundary and attach less to the counterbore wall. Above differences should result from the different configuration of the nozzle hole inlet passage. At the end of injection (the needle has closed), fuel drippings root from the residual fuel in the nozzle sac. Due to the smoother hole inlet, the fuel entering Hole-2 changes less in its flow direction and thus can maintain more momentum in the axial direction of the fuel streams together with a smaller level of dispersion. This may explain the less tip wetting in Hole-2.

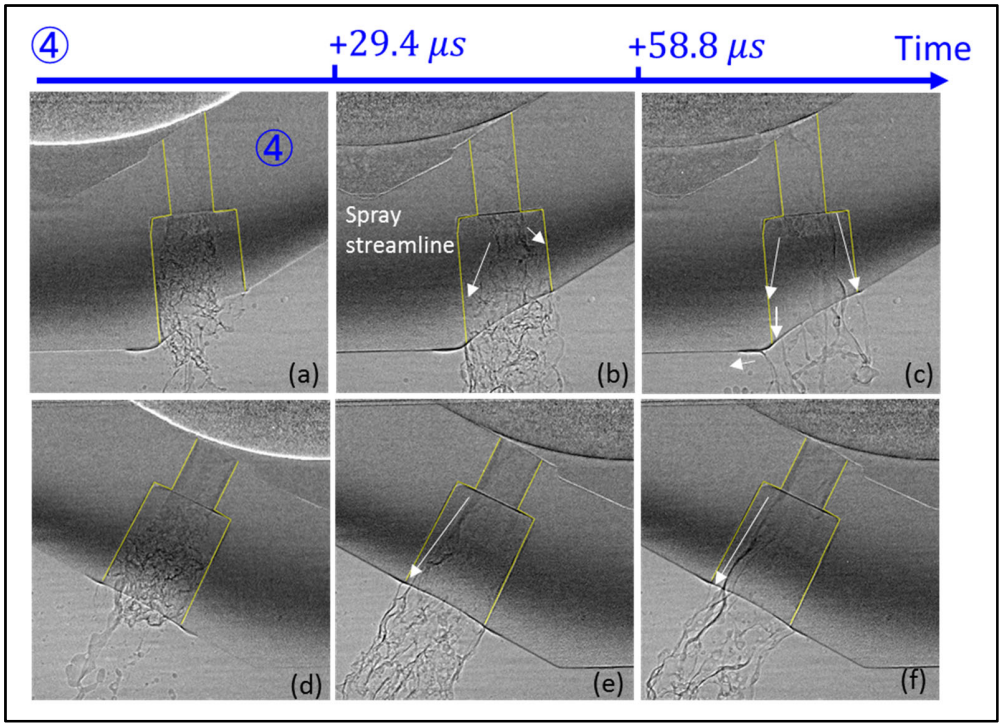

Figure 9. Comparisons of the tip wetting between the Hole-1 (a – c) and Hole-2 (d – f). Results are derived from the Ø0.30 mm nozzle and under an injection pressure of 4 MPa.

3.2.2 Effects of counterbore diameters on the nozzle tip wetting

In the section above, it has explained that the needle bouncing, injection pressure, and hole configuration can affect the formation of tip wetting, while the influence from the needle bouncing is the most critical. In this section, the counterbore diameter effect on tip wetting is discussed. Discussions are made in three periods separately, referring to during injection, during needle bouncing, and after the termination of the needle bouncing. First of all, Figure 10(b) shows that the tip wetting during injection (results in Period-1) is quite small and varies without a pattern as an increase in counterbore diameters. Regarding the tip-wetting increase during needle bouncing, it can be estimated by subtracting the results of Period-1 from Period-2, as the blue dash line shown in Figure 10(c). It is of particular interest that the tip wetting during needle bouncing increases slightly as the counterbore diameter increases from 0.25 mm to 0.40 mm and then decreases sharply from 0. 40 mm to 0.55 mm. After the needle bouncing terminates, it is observed that the residual fuel in nozzle sac still keeps flowing down along the counterbore wall (regarded as 'the drippings along counterbore walls'). This potential source to tip wetting can be estimated by subtracting the amount in Period-2 from Period-3, as the green dash-dot line shown in Figure 10(c). It is clear that the nozzle tip wetting due to the drippings along counterbore

walls decrease gradually as an increase of counterbore diameters. The final nozzle tip wetting of each nozzle depends on the combination of the processes described above, which results can be seen as the red solid line in Figure 10(c) (measured at Period-3). The final nozzle tip wetting reaches the maximum when the counterbore diameters of 0.30 mm and 0.35 mm are used. It is clear that the final nozzle tip wetting is dominated by the fuel drippings during needle bouncing because they have the most resembling tendency. An improved nozzle design to control the drippings flow against the counterbore and reduced needle bouncing could contribute to a less formation of tip wetting.

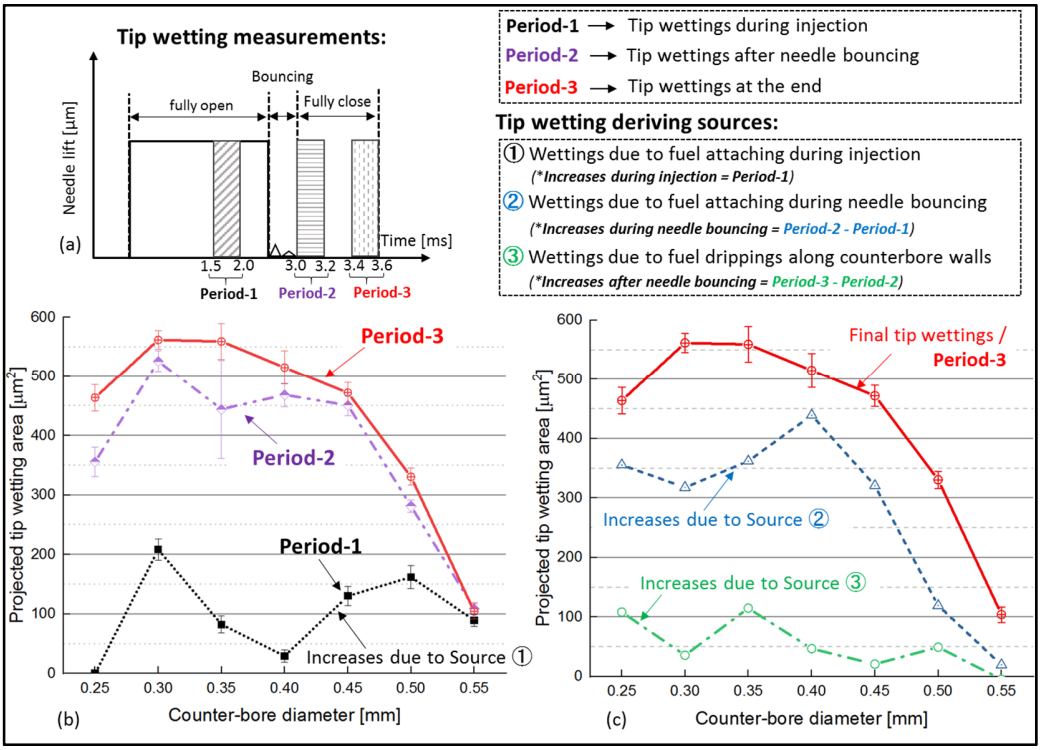

Figure 10. (a) Tip wetting measurements for a comparison of the counterbore-diameter effect. (b) Results of projected tip wetting areas measured at different periods. (c) An examination of the tip wetting deriving sources by using the results of (b).

Further discussions can be made on the features observed in Figure 10. First of all, during injection, the amount of tip wetting varies among the nozzles without a clear pattern. The potential reasons for this trend are considered below. First, the effect of counterbore diameters on the flow separation in the nozzle hole is examined. Figure 11(a) reveals that the flow separations are identical among the nozzles, indicating a similar flow dynamics in the nozzle hole and counterbore regardless of counterbore diameters. Figure 11(b-g) show further details that in the nozzle with a counterbore diameter of 0.25 mm, sprays hit the counterbore wall shortly

after leaving the nozzle hole, and no tip wetting is observed. It is considered that because the sprays spread little when the counterbore diameter is small, they hit the counterbore wall with strong momentum so that tip wetting can be flushed out. From the nozzle with a counterbore diameter of 0.30 mm, as shown in Figure 11(c) and (f), a clearance between the spray mainstream and the counterbore wall is observed, which might initiate the air entrainment into the counterbore so that the small-size droplets with low velocity can form tip wetting substantially. As the diameter further increases to 0.55 mm, as shown in Figure 11(d) and (g), the clearance between the spray and the counterbore wall further increases. However, individual droplets detached from the spray mainstream are observed and they still hit on the counterbore wall with the formation of tip wetting.

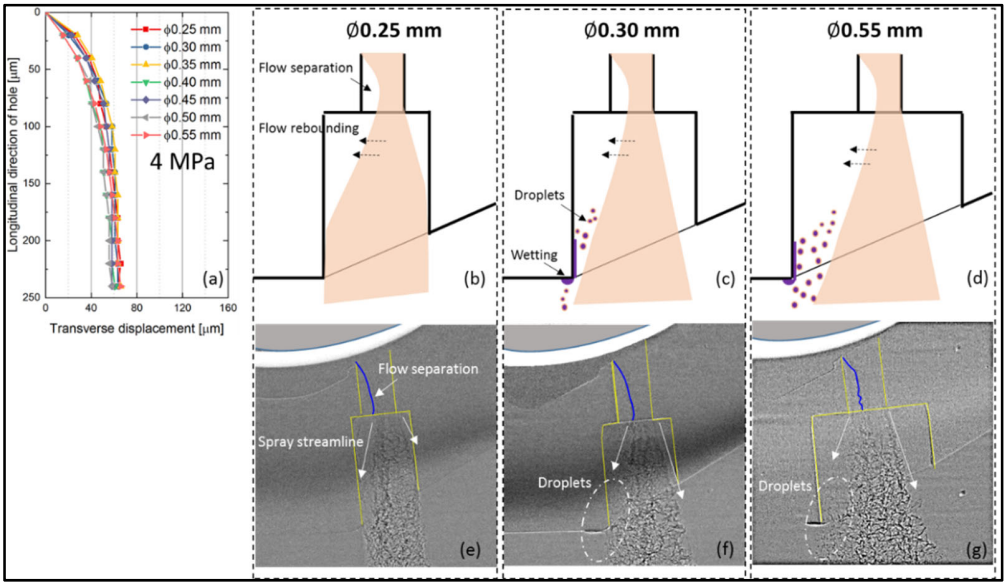

Figure 11. Counterbore diameter effect on the nozzle tip wetting during the injection: (a) flow separation profiles; (b-d) sketches of the flow pattern in small counterbore diameter and large counterbore diameter; (e-g) samples images (Results of the Hole-1 under the injection pressure of 4 MPa)

During needle bouncing, it is found in Figure 10(b) that tip wetting increases slightly from the counterbore diameter of 0.25mm to 0.40 mm, and then decreases sharply afterward from the counterbore diameter of 0.45 mm to 0.55 mm. The reasons are considered below. First of all, Figure 4 has shown that the nozzles have an identical amplitude of needle bouncing at the end of injection. Thus, it is excluded that the variance in nozzle tip wetting results from the different needle bouncing. Second, Figure 12(a-c) reveals that during the 1st and 2nd needle bouncing, the spray-like (left side) and ligament-like (right side) drippings occur, respectively. Based on our observations, two effects are coupled to decide the fuel drippings turning to tip wetting. When the counterbore diameter is small, drippings hit the counterbore wall quickly with relatively larger momentum due

to the fewer spreadings so that the wetting fuel can be flushed out, as illustrated in Figure 12(a). As the counterbore diameter increases, the momentum of fuel drippings at the instant of wall impingement attenuates due to the wider spreading of fuel drippings. As a result, fuel drippings can be more easily trapped on counterbore walls under the surface-tension effect. With a further increase in the counterbore diameter from 0.4 mm, tip wetting decreases sharply due to the increasingly fewer drippings hitting on counterbore walls, as depicted in Figure 12(c).

After the needle bouncing terminates fully, fuel still flows down along counterbore walls. However, tip wetting increases less at larger counterbore diameters, as shown in Figure 10(b). It is considered that this is because the larger counterbore diameter can provide the more wetting surface. Therefore, fuel is trapped on counterbore walls more due to the surface tension effect, resulting in the less tip wetting formed. In addition, it is noticed that *Oh et al.*[19] reported a suppressed tip wetting as the counterbore surface area decreases (equivalent to decreasing counterbore diameter in this study). Their conclusions slightly deviate from those of the current study, which shows a non-linear effect of counterbore diameter on tip wetting. The reason for this inconsistency is considered because in *Oh et al.*'s investigation only two nozzles with small counterbore diameter have been tested. The counter-diameter effect might have been revealed in a limited range.

Furthermore, it is noteworthy that the final nozzle tip wetting of each nozzle is determined by the nozzle tip wetting during the whole injection event, including the wetting during injection, the drippings during needle bouncing and the drippings after needle bouncing. It deserves further investigations to cover more influencing parameters and to achieve better understandings of the phenomenon, which benefit to propose the control strategies of tip wetting.

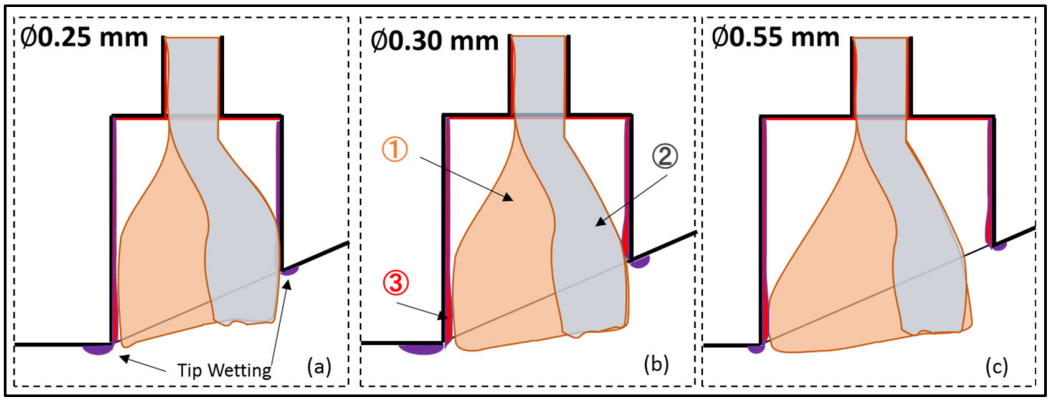

Figure 12. Counterbore diameter effect on the nozzle tip wetting at the end of injection: (a-c) sketches of the flow patterns of the nozzles. ① and ② represent spray-like drippings and ligament-like drippings, respectively.③ represents the drippings along counterball walls.

4. Conclusions

The nozzle tip wetting has been considered an important contributor to the particle emissions in GDI engines. In this study, tip wetting was examined in the real-size aluminum nozzles under the practical injection conditions of GDI engines. By taking advantages of the X-ray phase-contrast imaging technique, the needle motion and the transient flow characteristics inside nozzle holes and counterbores were visualized and quantified by parameters. A detailed analysis was conducted to understand the formation mechanism and influencing factors of tip wetting. The key conclusions of the current study can be summarized as below.

1. The needle bouncing, injection pressure, and hole configuration can affect the formation of tip wetting, while the influence from the needle bouncing is the most critical.
2. During needle bouncing, spray-like fuel drippings can be observed with a large amount. Once the drippings attach to counterbore walls, a significant increase in tip wetting occurs.
3. Increasing injection pressures can attenuate the needle bouncing and enhance the dripping momentum, resulting in a reduced tip wetting. In addition, the comparisons between Hole-1 and Hole-2 show that the suppressed flow separation in nozzle hole due to the different hole configuration can contribute to the concentrated drippings, leading to a less tip wetting formed.
4. Tip wetting slightly increases when the counterbore diameter changes from 0.25 mm to 0.35 mm and then decreases sharply afterward from 0.40 mm to 0.55 mm. This non-linear trend depends largely on the interaction between fuel drippings and counterbore walls during needle bouncing. It is discussed that two effects are coupled and responsible for the phenomenon, referring to the momentum of fuel drippings at the instant of wall impingement and the possibility for fuel drippings to interact with counterbore walls.

5. References

[1] Braisher M, Stone R and Price P. Particle number emissions from a range of European vehicles. SAE Technical Paper 2010-01-0786, 2010.

[2] Myung CL and Park S. Exhaust nanoparticle emissions from internal combustion engines: A review. *Int J Automot Technol* 2012; 13(1): 9-22.

[3] Moon S, Komada K, Sato K, Yokohata H, Wada Y and Yasuda N. Ultrafast x-ray study of multi-hole GDI injector sprays: effects of nozzle hole length and number on initial spray formation. *Exp Therm Fluid Sci* 2015; 68: 68-81.

[4] www.dieselnet.com/standards/eu/ld.php (2019) EU: Cars and Light Trucks. Available from: https://www.dieselnet.com/standards/eu/ld.php. (accessed 9 May 2019).

[5] www.transportpolicy.net/standard/china-light-duty-emissions (2019) China light-duty emissions. Available from: https://www.transportpolicy.net/standard/china-light-duty-emissions/. (accessed 9

403 May 2019).
404 [6] Wang C, Xu H, Herreros JM, Wang J and Cracknell R. Impact of fuel and injection system on
405 particle emissions from a GDI engine. *Appl Energ* 2014; 132: 178-191.
406 [7] Song H, Xiao J, Chen Y and Huang Z. The effects of deposits on spray behaviors of a gasoline
407 direct injector. *Fuel* 2016; 180: 506-513.
408 [8] Kazour J Befrui B, Husted H, Raney M, and Varble D. Innovative sprays and particulate reduction
409 with GDI injectors. SAE Technical Paper 2014-01-1441, 2014.
410 [9] Wang YH, Zheng R, Qin YH, Peng JF, Li MR, Lei JR, Wu YS, Hu M and Shuai SJ. The impact of
411 fuel compositions on the particulate emissions of direct injection gasoline engine. *Fuel* 2016;
412 166: 543-552.
413 [10] Peterson K and Grover R. Application of optical diagnostics and simulation to fuel injector tip
414 wetting and soot production. *Proceeding of the 11th International Symposium on Combustion*
415 *Diagnostics*, Beiträge, Baden-Baden, Germany, July 1-2, 2014.
416 [11] Oude ND, Freeland P, Behringer M and Aleiferis P. Developing Low Gasoline Particulate
417 Emission Engines Through Improved Fuel Delivery. SAE Technical Paper 2014-01-2843, 2014.
418 [12] Berndorfer A, Breuer S, Piock W and Bachi PV. Diffusion Combustion Phenomena in GDi Engines
419 caused by Injection Process. SAE Technical Paper 2013-01-0261, 2013.
420 [13] Parsons D, Akehurst S and Brace C. The potential of catalysed exhaust gas recirculation to
421 improve high-load operation in spark ignition engines. *Int J Engine Res* 2015; 16(4): 592-605.
422 [14] Wang B, Jiang Y, Hutchins P, Badawy T, Xu H, Zhang X, Rack A and Tafforeau P. Numerical
423 analysis of deposit effect on nozzle flow and spray characteristics of GDI injectors. *Appl Energ*
424 2017; 204: 1215-1224.
425 [15] Leach F, Knorsch T, Laidig C and Wiese W. A review of the requirements for injection systems
426 and the effects of fuel quality on particulate emissions from GDI engines. SAE Technical Paper
427 2018-01-1710, 2018.
428 [16] Befrui B, Corbinelli G, D'Onofrio M and Varble D. GDI multi-hole injector internal flow and
429 spray analysis. SAE Technical Paper 2011-01-1211, 2011.
430 [17] Knorsch T, Rogler P, Miller M and Wiese W. On the evaluation methods for systematic further
431 development of direct-Injection nozzles. SAE Technical Paper 2016-01-2200, 2016.
432 [18] Dageförde H, Kiefer A, Samenfink W, Wiese W, and Kufferath A. Requirements for spray and tip
433 design of a multi-hole injector for DISI engines. *International Conference On Liquid Atomization*
434 *And Spray Systems*, Tainan, August 23-27, 2015.
435 [19] Oh HC, Lee JH, Han SK, Park CS, Bae CS, Lee JH, Lee JH, Seo IK and Kim SJ. Effect of injector
436 nozzle hole geometry on particulate emissions in a downsized direct injection gasoline engine.
437 SAE Technical Paper 2017-24-0111, 2017.
438 [20] Fischer A and Marina T. Methodology and tools to predict GDI injector tip wetting as predecessor
439 of Tip Sooting. SAE Technical Paper 2018-01-0286, 2018.
440 [21] Endrizzi M. X-ray phase-contrast imaging. *Nuclear Inst. and Methods in Physics Research, A* 2018;
441 878: 88-98.
442 [22] Lee WK, Fezzaa K and Wang J. Metrology of steel micronozzles using x-ray propagation-based
443 phase-enhanced microimaging. *Appl. Phys. Lett.* 2005; 87:084105.
444 [23] Moon S, Tsujimura T, Gao Y, Park S, Wang J and Kurimoto N. Biodiesel effects on transient needle
445 motion and near-exit flow characteristics of a high-pressure diesel injector. *Int J Engine Res* 2013;
446 15: 504-18.
447 [24] Huang WD, Moon S and Ohsawa K. Near-nozzle dynamics of diesel spray under varied needle lifts
448 and its prediction using analytical model. *Fuel* 2016; 180: 292-300.
449 [25] Huang WD, Moon S, Gao Y, Li ZL and Wang J. Eccentric needle motion effect on near-nozzle
450 dynamics of diesel spray. *Fuel* 2017; 206: 409-419.

[26] Huang WD, Moon S, Gao Y, Wang J, Ozawa D and Matsumoto A. Hole number effect on spray dynamics of multi-hole diesel nozzles: an observation from three-to nine-hole nozzles. *Exp Therm Fluid Sci* 2019; 102: 387-396.
[27] Moon S, Gao Y, Wang J, Fezzaa K and Tsujimura T. Near-field dynamics of high-speed diesel sprays: Effects of orifice inlet geometry and injection pressure. *Fuel* 2014;133:299-309.
[28] Moon S, Gao Y, Park SP, Wang J, Kurimoto N and Nishijima Y. Effect of the number and position of nozzle holes on in- and near-nozzle dynamic characteristics of diesel injection. *Fuel* 2015; 150: 112-122.
[29] Piehl JA, Zyada, A, Bravo L, and Samimi-Abianeh O. Review of oxidation of gasoline surrogates and its components. *Journal of Combustion* 2018:8406754.
[30] Itaya T, Kumano K, Maekawa N, Oosuga M, Ogura K, Miyake T, Yasukawa Y and Yoshimura K. Study of a particle number reduction method using flow analysis of fuel injectors. *Transactions of JSAE* 2018; 49(2): 181-186. (In Japanese)